# Statistical Analysis of fMRI using Wavelets: Big Data, Denoising, Large-p-Small-n Matrices

Sam Efromovich*

**Article Type:**

Overview

**Abstract**

Over the past decade functional Magnetic Resonance Imaging (fMRI) has been intensively used to study the complex functional network organization of the human brain and how it changes in time. An fMRI machine produces 3-D time-course cerebral images that contain hundreds of thousands of voxels and each voxel is scanned for hundreds of times. This potentially allows the researchers to explore functional connectivity on a voxel-to-voxel level, and also yields a number of serious statistical complications. First of all, the high-dimension property of fMRI data turns it into Big Data. Further, the study of functional brain network for so many voxels involves the problem of estimation of and simultaneous inference for large-p-small-n cross-covariance matrices. Further, all problems should be solved in the presence of notoriously large fMRI noise which often forces statisticians to average signals over large areas instead of considering a network between individual voxels. An attractive alternative to the averaging, discussed in the paper, is a multiresolution wavelet analysis complemented by special procedures of estimating noise and estimation and simultaneous inference for cross-covariance and cross-correlation matrices for hundreds of thousands pairs of voxels, and it is fair to say that if wavelets have not been already known, fMRI applications would necessitates their creation. Both task and resting-state fMRI are considered, and lessons from the wavelet analysis of ultra-fast and conventional neuroplasticity fMRI experiments are presented. The article is self-contained and does not require familiarity with wavelets or fMRI.

*Department of Mathematical Sciences, The University of Texas at Dallas, Richardson, TX 75080, USA

# INTRODUCTION

Many brain diseases, such as Alzheimer's and Parkinson's diseases, Attention Deficit Hyperactive Disorder, Epilepsy, Schizophrenia, Depression and Anxiety, have been shown to be related to brain connectivity networks. Further, potential treatments of these diseases and post-stroke complications may be found via understanding of how human brain functional connectivity changes during experimental studies. See a discussion and reviews of available literature in Anderson et al. (2010), Dimyan and Cohen (2011), Skidmore (2011), Faust et al. (2015), Wee et al. (2016), Laird et al. (2017), Xue et al. (2017), and Papoutsi et al. (2018). Further, the study of connectivity in healthy brain function is important topic in network neuroscience, see a discussion and reviews in Honey et al. (2007), Bassett et al. (2011), Goni et al. (2014), Sporns (2014), Thomas et al. (2014), Misic and Sporns (2016), Bassett and Sporns (2017), Laird et al. (2017), and Mill et al. (2017).

Functional Magnet Resonance Imaging (fMRI) is a non-invasive technique for mapping brain functions using blood-oxygenation-level-dependent (BOLD) contrasts. Its traditional task is to detect brain areas activated by a stimulus, and the latter is a challenging problem due to large noise and artifacts present in the data. Statistical analysis of fMRI is a familiar topic in the literature with the main emphasis on a conventional problem of denoising images. See a discussion in Logothetis et al. (2001), Lazar (2008), Lindquist (2008), Valdez-Jasso (2010) and Ashby (2011).

Over the last decade, fMRI has been intensively used for analysis of functional connectivity which defines pathways between brain regions that share functional properties and traditionally defined via correlation between spatially remote neurophysiological events. Regions of the brain do not have to be structurally (physically or anatomically) connected to have functional connectivity, and a structural connection does not necessarily signify a functional link. An example of functional connectivity between left and right motor cortices will be presented shortly. fMRI may be used to study the brain functional connectivity based on the induced stimulus by a task (task fMRI) or during a task-free experiment (resting-state fMRI). Task fMRI is interested in dynamic of the connectivity during a sequence of short resting and task (stimulus) performing periods. The aim of resting-state fMRI is in mapping

the network behavior and study large-scale brain segregations and integrations that occur due to the human brain ability to organize spontaneous fluctuations in the resting state. While task and resting-state fMRI present many identical neuroscience challenges, they also have fundamental differences that are reflected in statistical analysis (Di et al. 2013, Zhang, S. et al. 2016, Mwansisya et al. 2017). For instance, in wavelet analysis different wavelet transforms are recommended.

The paper is primarily devoted to explanation of the wavelet analysis of fMRI data. The reader does not need to be familiar with either wavelets or fMRI. All required basics will be explained in the next section via discussion of a special Ultra Fast fMRI experiment. This section also sheds light on observed BOLD signals and large noise in conventional fMRI data. Then next 3 sections are devoted to explanation of wavelet statistical analysis, including evaluation of the noise level and estimation of and inference for large-p-small-n cross-covariance and cross-correlation matrices. The results are illustrated via a task fMRI study of neural plasticity. The final section is devoted to specifics of the resting-state fMRI.

## ULTRA FAST TASK fMRI

The main goal of fMRI is to locate, map, and analyze neurons activity in the brain. A conventional explanation of how MR scanner detects activity of neurons is as follows. Neurons consume oxygen which is attached to hemoglobin molecules in the blood. When activity of a neuron increases, it demands more oxygen which is locally delivered by increased flow of blood. The supply of oxygen is always larger than the demand and this yields an increased blood oxygen concentration near activated neurons. MR scanner can measure the change in oxygenated blood due to the following phenomenon. Oxygen attached to the hemoglobin molecule shields an iron atom and this makes the hemoglobin molecule almost magnetically inactive. If oxygen is not attached, the hemoglobin's iron makes the molecule paramagnetic. This is the phenomenon which is used by MRI which allows us to analyze the Blood Oxygen Level Dependent (BOLD) signal/effect rather then underlying activity of neurons. At the same time, via simultaneous measurement of BOLD and electrical effects, it has been verified that BOLD can be used to measure activity of neurons, see a discussion in Logothetis et al.

(2001), Lazar (2008) and Ashby (2011).

Instead of going into details of fMRI, for our purposes it is better to explain everything via a special Ultra Fast (UF) fMRI experiment when just one slice of human brain is screened. The experiment was conducted by the UTSouthwestern medical school, see Valdez-Jasso (2010). To detect brain activity, a participant is placed in the MR scanner and a visual stimulus is used to activate neurons. During the first 15 seconds the patient is at rest. After the rest, 5 seconds of visual stimulation, done by flash check board, are followed by 30 seconds of rest. Then this 5-30 seconds pattern of activation-rest is repeated. UF fMRI uses a single slice of visual cortex to acquire BOLD signal every 50 milliseconds. The available fMRI data are preprocessed using the standard software AFNI that removes effects of head movement and physiological fluctuations in the signal time course, see Lazar (2008) and Caballero-Gaudes and Reynolds (2017). However, as we will see shortly, the preprocessing is not perfect and we still observe physiological and MR induced components in the BOLD signals.

For each voxel from the slice the measured BOLD signal is an equidistant time series

$$Y(t_l) = f(t_l) + \tau\epsilon_l, \quad t_l = \delta l, \ \ l = 1, 2, \ldots, n. \tag{1}$$

Here $f(t)$ is a deterministic signal which may be written as the sum of a hemodynamic response to visual stimuli (the component/signal of interest) plus unfiltered physiological signals (like cardiac and respiratory) and drift (trend), $\delta$ is the period of collecting data, $\epsilon$ is additive zero-mean and unit variance noise, and $\tau$ is the standard deviation of the fMRI noise. Note that both $f$ and $\tau$ are specific for each voxel. As we will see shortly, the very small period $\delta$ in the UF fMRI allows us to zoom in on signals produced by MRI. We can also refer to the time series as equidistant regression with $f(t) = \mathbb{E}\{Y(t)\}$ and $\tau\epsilon$ being regression error, see Efromovich (1999a). Because no information about shape of an underlying signal $f$ is available (after all, finding shapes is the main aim of the experiment), it is natural to use an adaptive nonparametric curve estimation which is based solely on data and requires neither information about shape/smoothness of $f$ nor a manual adjustment of estimators, see Efromovich (1999a,2018a).

For the considered setting, due to large number of observations and inhomogeneity of

estimated signals, it is natural to use a series estimation based on wavelet bases because wavelets are created for approximation of such signals. A thorough discussion of wavelets and estimation procedures can be found in books Ogden (1997), Efromovich (1999a), Vidakovic (1999) and Nason (2008). To briefly describe a procedure, let us for simplicity assume that $n$ is dyadic. Then an estimated signal $f$ can be approximated by a wavelet series with $n$ terms,

$$f'(t) = \sum_{k=0}^{n/2^J} s_{Jk}\phi_{Jk}(t) + \sum_{j=1}^{J}\sum_{k=0}^{n/2^j} d_{jk}\psi_{jk}(t). \tag{2}$$

Here $J$ is the number of used multiresolution components (scales). For our data we choose $J = 9$ and this recommendation will be explained shortly. Functions $\phi_{jk} = 2^{-j/2}\phi(2^{-j}t - k)$ and $\psi_{jk} = 2^{-j/2}\psi(2^{-j}t - k)$ are orthonormal and generated by dilation and translation of a scaling function $\phi$ (also referred to as father wavelet) and a wavelet function $\psi$ (also referred to as mother wavelet). A scale function is integrated to one and a wavelet function is integrated to zero. Further, $s_{jk} = \int_{-\infty}^{\infty} f(t)\phi_{jk}(t)dt$ and $d_{jk} = \int_{-\infty}^{\infty} f(t)\psi_{jk}(t)dt$ in (1) are wavelet coefficients. There are many wavelet bases to choose from; see Vidakovic (1999) and Nason (2008). To be specific, here wavelet basis Coiflet 5 is used.

For observed time series $Y_1, \ldots, Y_n$ any wavelet software (R and MATLAB are more popular sourses) allows one to calculate via a discrete wavelet transform (DWT) empirical wavelet coefficients $\{\tilde{s}_{jk}, \tilde{d}_{jk}\}$ which are unbiased estimates of underlying wavelet coefficients in (2). Next step is to estimate underlying wavelet coefficients by an estimator $\{\hat{s}_{jk}, \hat{d}_{jk}\}$. Here adaptive nonparametric estimator of Efromovich (1999b), available in R software Efromovich (1999a), is used. This estimator combines excellent asymptotic properties for vast classes of inhomogeneous functions with a reliable denoising for relatively small sample sizes. The estimator uses unchanged empirical scaling coefficients $\hat{s}_{jk} = \tilde{s}_{jk}$ and it shrinks empirical wavelet coefficients $\hat{d}_{jk} = \lambda_{jk}\tilde{d}_{jk}$ using data-driven shrinkage weights $\lambda_{jk} \in [0, 1]$. Calculation of shrinkage weights is rather involved, and description of the procedure is skipped here because it can be found in the above-mentioned references. Finally, the denoised signal (estimated regression function) can be written as

$$\hat{f}(t) = \sum_{k=0}^{n/2^9} \hat{s}_{9k}\phi_{Jk}(t) + \sum_{j=1}^{9}\sum_{k=0}^{n/2^j} \hat{d}_{jk}\psi_{jk}(t). \tag{3}$$

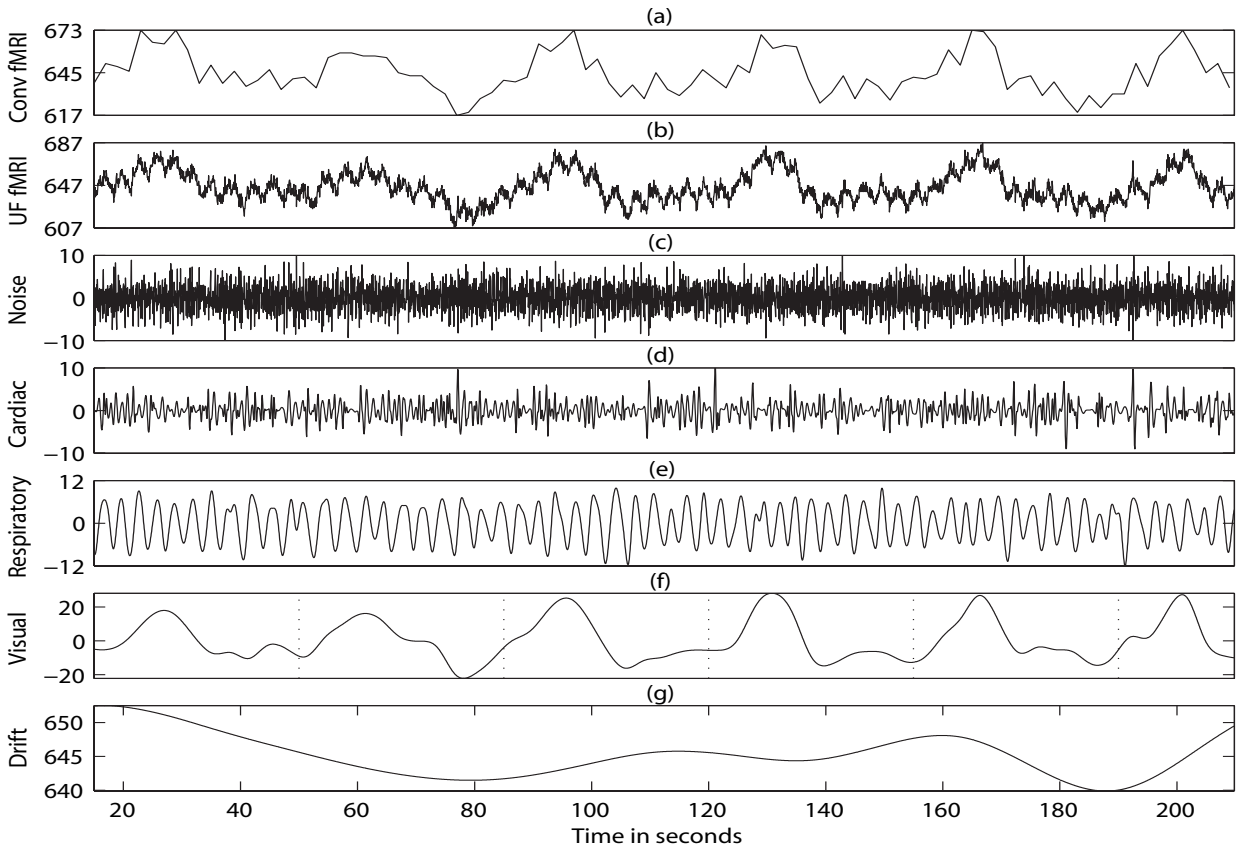


Figure 1: Wavelet multiresolution decomposition of fMRI signal. Diagram (a) shows data for a particular voxel which is scanned with the period of 2 seconds. Diagram (b) shows data for the same voxel with the period of 50 milliseconds. Diagrams (c)-(g) exhibit results of the wavelet multiresolution analysis of the signal shown in diagram (b). Diagram (c) shows fMRI noise, diagram (d) shows cardiac signal, diagram (e) shows respiratory signal, diagram (f) shows the hemodynamic response to visual stimuli, and diagram (g) shows the fMRI drift. The vertical dotted lines in the diagram (f) show times of the visual stimulus activation.

Figure 1 presents multiresolution analysis of observed UF fMRI signal for a voxel in visual cortex. Observations (1) are shown in diagram (b). Here we are dealing with a pronounced signal which may be recognized despite the highly fluctuated noise. To get an idea how a signal for this voxel could look like if a conventional fMRI was used which scans many slices, the top diagram (a) exhibits the same signal where now every 40th observation is shown, that is, images are taken every other second. A visual stimulus activates neurons

and this triggers a process of blood oxygenation/deoxygenation measured by MR scanner, and it may be expected to see a pronounced hemodynamic response function. Let us check how the proposed wavelet analysis highlights the hemodynamic response and separates it from nuisance components of the observed BOLD signal. Diagrams (c)-(g) show how the adaptive wavelet estimator (3) performs. Let us describe these 5 diagrams in turn beginning with the bottom diagram (g) showing the *Drift* (D) which is also may be referred to as the trend. This component reflects a slowly changing level of blood oxygenation/deoxygenation due to neuronal activity as well as due to possible slow changes in the MR scanner. This component is present even if the brain is rested, its formula is $\hat{f}_D(t) = \sum_{k=0}^{n/2^9} \hat{s}_{9k}\phi_{9k}(t)$, and we also see the drift in (3). In the terminology of a wavelet multiresolution analysis, drift is the *smooth* component defined by estimated coefficients for scale functions on the coarsest (here number 9) scale. Let us also note that drift removes a constant shift — all other components of the multiresolution analysis are integrated to zero. Diagram (f) shows us the hemodynamic response of neurons to visual stimuli, this is the primary signal of interest and it is called *Visual Response* (VR) in Valdez-Jasso (2010). This component is defined as

$$\hat{f}_{VR}(t) = \sum_{j=7}^{9} \sum_{k=1}^{n/2^j} \hat{d}_{jk}\psi_{jk}(t). \tag{4}$$

Note that the hemodynamic response to visual stimuli is defined by 3 coarsest scales of the wavelet function $\psi$. The VR looks like a detrended and then correctly smoothed version of the conventional fMRI signal shown in the top diagram (a). Let us explain why VR occupies 3 coarsest wavelet scales. Recall that each session has 5 seconds of visual stimulation and 30 seconds of rest, and this creates the frequency pattern of VR and the corresponding wavelet scales. Also note that the periodic structure of VR is clearly seen in diagram (f). Further, it is easy to notice that a particular shape of VR changes from one session to another. Further, according to Valdez-Jasso (2010) dramatic changes in hemodynamic responses of participants were observed when taken at different days.

Diagram (e) shows us the *Respiratory* (R) activity. This is a physiological component occurring on frequencies of breathing and this explains the name. Respiratory component is

defined as

$$\hat{f}_R(t) = \sum_{j=5}^{6} \sum_{k=1}^{n/2^j} \hat{d}_{jk} \psi_{jk}(t). \tag{5}$$

Let us note that for a conventional fMRI, with the period of scanning in seconds, the respiratory signal cannot be observed and will be part of a noise. This is one of the reasons why UF fMRI is so instructive and sheds light on wavelet multiresolution analysis of fMRI.

Now let us return to visualization of diagrams (a) and (e)-(f). Note that magnitude of the respiratory signal (e) is comparable with the hemodynamic response shown in diagram (f). This is what explains a traditional sawlike shape of the curve in diagram (a). Diagram (d) shows us *Cardiac* (C) activity. This is another physiological periodic component of UF fMRI signal which occurs with the frequency of heart beats,

$$\hat{f}_C(t) = \sum_{j=3}^{4} \sum_{k=1}^{n/2^j} \hat{d}_{jk} \psi_{jk}(t). \tag{6}$$

For a conventional fMRI this component will be a nuisance, but it is nicely visualized in denoised UF fMRI data. Finally, diagram (c) exhibits the *Noise* which is the total of signals on the two finest scales. It represents the fMRI noise. As we see, the noise is relatively large even when it is separated from physiological components. As about its distribution, Valdez-Jasso (2010) shows that a typical Noise component is either white Gaussian or short-memory Gaussian.

Now we are in a position to return to the problem of choosing the number $J$ of multiresolution components. As we see from Figure 1, a good choice of $J$ allows us to observe a signal of interest (here the hemodynamic response) on scales separated from scales where nuisance signals are located. Because all scales correspond to specific frequencies, knowing typical frequencies for all involved signals is paramount in choosing the number of multiresolution components.

Another important observation, related to the topic of Big Data (see a discussion of fMRI Big Data in Fan, Han and Liu 2014), is about data-compression property of the used wavelet estimator. For the studied data $n = 4096$ and the total number of non-zero wavelet coefficients in the estimate (3) is 256. Specifically, 8, 27, 85 and 136 wavelet coefficients define the Drift, Visual Response, Respiratory and Cardiac components, respectively. Similar

numbers are observed for other voxels. The conclusion is that the elaborate Visual Response is described by just 27 coefficients instead of 4096 underlying observations.

**Lessons of UF fMRI for conventional fMRI**. Conventional fMRI periodically screens a large number of slices and, depending on the number of slices, for a particular voxel the period may be from 0.5 to 2 seconds. For the period of 2 seconds, the reader may compare signals (a) and (b) in Figure 1. The increased period clearly creates a number of problems with the main one being estimation of the noise, and this jargon means estimation of parameter $\tau$ in (1). A traditional wavelet estimator considers a signal at the first scale as a white Gaussian noise with the standard deviation equal to $\tau$. This is the idea of the *mad* (sample median recalculated into standard deviation) procedure recommended in the wavelet literature and supported by all wavelet softwares, see Efromovich (1999a) and Nason (2008). This approach is valid for UF fMRI when signals are measured every 50 milliseconds, but let us explain what happens for a conventional fMRI. The frequency of collecting data is about $2^5$ to $2^6$ times less frequent, and hence for conventional wavelet analysis the first scale will combine everything from scale 1 to scales 5 or 6 for UF fMRI. Returning to Figure 1 and formulas (5) and (6), we may conclude that both the respiratory and cardiac signals will be present on scale 1. One possible remedy is to reduce number of slices and screen voxels more frequently, see Henson et al. (1999) and Smith et al. (2015), but still physiological components will be present on scale 1. As a result, a lot of attention in the literature has been devoted to reducing the deterministic physiological noise via technological, bioengineering and statistical improvements, see Lazar (2008), Welvaert and Rosseel (2013), Patel et al. (2016) and Azmen and Azsen (2018).

Another important lesson of the UF fMRI, discussed in Valdez-Jasso (2010), is that physiological components observed at different voxels, while originated by the same deterministic sources, are not the same and not even scale-location transformations of each other. At the same time, geometrically close voxels have a larger likelihood to exhibit similar physiological patterns.

Finally, UF fMRI shows that the standard deviation $\tau$ of the pure MR noise is not the same for all voxels, in other words, each voxel may have its own $\tau$. This is a complication that will be addressed shortly.

# NEUROPLASTICITY EXPERIMENT AS EXAMPLE OF CONVENTIONAL TASK fMRI

Neuroplasticity, also known as brain plasticity and neural plasticity, is the ability of the brain to change throughout an individual's life, e.g., brain activity associated with a given function can be transferred to a different location. There has been a growing interest in using fMRI to study neuroplasticity, see a discussion in Thomas et al. (2007), Dimyan and Cohen (2011), Sharma, Classen and Cohen (2013), Faivre et al. (2015), Pantano et al. (2015), and Papoutsi et al. (2018).

Following Tung et al. (2013), let us present an example of a conventional task fMRI neuroplasticity experiment that will help us to explain wavelet analysis and its challenges. The aim of experiment was to study changes in connectivity between left and right motor cortices after right-hand button clicking training sessions, and it was conducted on twenty-four healthy right-handed adult volunteers (participants) by the University of Texas Southwestern Medical Center. Note that the left hemisphere (its motor cortex) is in charge of the right hand, and it is of interest to understand the reaction (if any) of the right hemisphere. The experiment included three scan runs: (1) A five-minute pre-training fMRI run when a participant was instructed to just look at a white crosshair. Due to the five minute time and the repetition time of 1 second, 300 observations of the BOLD signal were obtained for each voxel; (2) A twenty-three-minute motor task period when a volunteer was asked to press by a right-hand thumb a button three times when the color of the cross-hair changed. The color change occurred every 27-32 seconds randomly and there were 40 stimulations. The motor task period was divided into 4 parts and 340 observations of the BOLD signal were obtained for each part. (3) A five-minute post-training fMRI run when a volunteer was instructed to just look at a white crosshair. 21 axial slices were periodically screened and this yielded repetition time, which is the time between successive scans of the particular volume of tissue, of 1 second. Overall, 300 observations of the BOLD signal were obtained for each voxel per each run. Further, available fMRI data were preprocessed using the standard software AFNI and physiological fluctuations in the signal time course were removed by regressing out time courses of the whole brain white matter, cerebral spinal fluid, and six motion vectors (Tung

et al. 2013, Caballero-Gaudes et al 2017).

Now let us summarize information available for statistical analysis. For 1000 voxels in each hemisphere, we have time series of BOLD signals for: pre-training (resting) run with 300 observations; four motor-task parts with 340 observations per part; post-training (resting) run with 300 observations.

Because of the large number of interhemispheric voxel-pairs and large fMRI noise, a standard and well accepted solution is based on averaging time series of images in each hemisphere, calculating correlations for average images in pre- and post-training runs, and then using a paired t-test for the 24 participants. The t-test supported a conjecture about the increase in correlation after training sessions among the 24 participants and, as a result, supported the conjecture about the brain plasticity (Tung et al. 2013). On the other hand, the averaging made it impossible to study brain connectivity on voxel-to-voxel level.

# WAVELET DECOMPOSITION FOR PLASTICITY EXPERIMENT

Efromovich and Smirnova (2014) made an attempt to analyze the plasticity fMRI data via a wavelet approach on a voxel-to-voxel level.

For a particular voxel the BOLD signal is observed every second with 300 observations for the pre- and post-training fMRI runs, and 340 observations for the training runs. The used Discrete Wavelet Transform (DWT) is based on a dyadic number $n$ of observations, and hence we choose $n = 256 = 2^8$ observations for each run (it will be explained later how to use all observations). Further, following Efromovich (1999a) we rescale signals for all runs onto the unit interval $[0, 1]$. Then an observed continuous BOLD signal $\tilde{Y}(t)$, $t \in [0, 1]$ for an fMRI run may be written as

$$\tilde{Y}(t) = \sum_{k=1}^{n/2^5} \tilde{s}_{5k}\phi_{5k}(t) + \sum_{j=1}^{5}\sum_{k=1}^{n/2^j} \tilde{\theta}_{jk}\psi_{jk}(t). \tag{7}$$

Here five wavelet scales are used in the decomposition, and this choice will be explained shortly.

Now we are in a position to explain how the wavelet expansion (7) allows us to define the motor-response (MR) BOLD-component of interest which reflects either a neuron activity during pre- or post-training runs or a hemodynamic response during training runs (the motor signal). First, let us look at this issue via a traditional frequency approach, and then comment on it via our experience with the UF fMRI. Each scale $j$ in a wavelet multiresolution decomposition corresponds to a specific frequency. In our case, because a signal is observed every second, the corresponding frequency of each scale is $2^{-j}$. As a result, the frequency of the first scale is 0.5 Hz, the second is 0.25 Hz, the third is 0.125, etc. During rest runs, the traditional frequency bandpass for the BOLD-component of interest is 0.01-0.1 Hz, while hemodynamic responses during training runs last 15-20 seconds and the stimuli occur every 27-32 seconds (Lazar 2008, Birn 2012, Tung et al. 2013). As a result, the observed MR BOLD-component of interest may be written as a combination of scales 3, 4 and 5, namely

$$\tilde{f}_{MR}(t) := \tilde{B}(t) := \sum_{j=3}^{5} \sum_{k=1}^{n/2^j} \tilde{\theta}_{jk} \psi_{jk}(t). \tag{8}$$

This definition also follows from our previous UF fMRI analysis because in the plasticity experiment the frequency of measurements for each voxel is 20 times slower, and this is why in (8) everything shifts 4 scales down with respect to (4). The presented analysis explains the choice of five wavelet scales.

Empirical wavelet coefficients $\tilde{\theta}_{jk}$ are contaminated by noise. Namely, if

$$B(t) = \sum_{j=3}^{5} \sum_{k=1}^{n/2^j} \theta_{jk} \psi_{jk}(t) \tag{9}$$

is the underlying BOLD-component of interest, then

$$\tilde{\theta}_{jk} = \theta_{jk} + n^{-1/2} \tau \xi_{jk}. \tag{10}$$

Here $\xi_{jk}$ is a standard Gaussian random variable, $n^{-1/2}\tau\xi_{jk}$ is the empirical fMRI wavelet noise, and the reader may compare (10) with (1).

As we already know, the low-frequency component $\sum_{k=1}^{n/2^5} \tilde{s}_{5k} \phi_{5k}(t)$ represents the fMRI background drift and is not of interest to us. Now let us turn our attention to the first two wavelet scales. As we already know from the UF fMRI wavelet analysis, these two

scales are now combine together all unfiltered physiological fluctuations and the empirical fMRI noise of interest. We may also understand this from the frequency analysis. The frequency of physiological fluctuations is typically greater than 0.2 Hz (Barrett et al. 2016), and this is why these fluctuations are captured by the two finest scales. While we are not interested in the signals on the two finest scales per se, the first scale is traditionally used to estimate parameter $\tau$ by the above-mentioned procedure *mad*. Unfortunately, as it is shown in Efromovich and Wu (2018), using this standard procedure significantly overestimates the noise due to the presence of physiological components. The next section explains how this issue may be resolved via taking into consideration the presence of relatively large physiological components.

# ESTIMATION OF NOISE IN CONVENTIONAL fMRI

In the wavelet context, the phrase "estimation of noise" means that we would like to estimate the standard deviation $\tau$ of the noise in model (1) or equivalently in model (10). The problem has a simple solution, via the *mad* procedure, for UF fMRI where the first scale contains only the empirical noise, but as we also know it becomes extremely challenging for conventional fMRI due to the presence of unfiltered physiological components on the first scale, see a discussion in Chang and Glover (2009), Weissenbacher et al. (2009), Birn (2012), He and Liu (2012), Welvaert and Rosseel (2013), Murphy, Birn and Bandettini (2013) and Caballero-Gaudes and Reynolds (2017). A traditionally used approach is to assume that everything is filtered out and then use *mad* for the first scale, see reviews in Efromovich and Smirnova (2014), Smith et al. (2015), Patel and Bullmore (2016), Zhang, Z. et al. (2016), Preti et al. (2017). The consequences are that the estimated $\tau$ may be dramatically larger than an underlying one, and this may prevent us from feasible statistical analysis of neuron connectivity on voxel-to-voxel level because a majority of active pairs of voxels will be declared as nonactive. Further, a larger noise yields oversmoothed estimated signals, and interesting examples and a discussion may be found in Efromovich and Wu (2018).

Now let us explain how the problem of estimation of the noise in the presence of a deterministic additive component, like an unfiltered physiological signal, may be solved. The

underlying idea is that, according to the lessons of UF fMRI, for an active voxel there may be a geometrically close voxel with a similar deterministic additive component. Using this fact we can regress finest scales of one voxel on another and then estimate $\tau$. Let us explain this solution more formally for the plasticity example. Denote by $\tilde{Y}'_l := \sum_{j=1}^{2}\sum_{k=1}^{n/2^j}\tilde{\theta}_{jk}\psi_{jk}(l/n)$ the sum of first and second wavelet scales for a voxel of interest, and by $Y'_l := \sum_{j=1}^{2}\sum_{k=1}^{n/2^j}\theta_{jk}\psi_{jk}(l/n)$ the corresponding underlying deterministic component, $l = 1, \dots, n$. According to the above-presented explanation, the deterministic component may be explained by physiological factors and hence it should be close to the deterministic component $X'_l$ of a nearby voxel, more precisely it is reasonable to assume that $Y'_l = \beta X'_l$ (note that signals on the first and second scales are integrated to zero so there may be only the scale/slope term $\beta$ in the relation). As a result, we may regress the observed $\tilde{Y}' := \{\tilde{Y}'_l, l = 1, 2 \dots, n\}$ on the observed $\tilde{X}' := \{\tilde{X}'_l, l = 1, 2, \dots, n\}$. Note that here we are dealing with the regression where the predictor is also observed with errors, the regression errors are of the primary interest, and we can estimate the standard deviation $\tau$ of the regression error as explained in Efromovich (1999a) and Casella and Berger (2002). We know from UF fMRI that the closer two voxels are, the more similar the physiological components are. In order to avoid the slice timing issue and to align with the assumption, it is suggested to choose a "nearby" voxel as the one with largest correlation among the $3 \times 3$ vicinity within the same slice. Let us also note that the choice of a larger vicinity, tested in simulations and on real data in Efromovich and Wu (2018), made no difference.

# ESTIMATION OF CROSS-COVARIANCE MATRICES

Estimation of large-p-small-n sparse covariance matrices is one of the hottest topics in modern statistics, and in part it is motivated by the exponentially growing microarray's applications. If $\mathbf{X} := (X_1, \dots, X_p)$ is a p-variate random vector and given a sample $\mathbf{X}_1, \dots, \mathbf{X}_n$, the problem is to estimate the covariance matrix of $\mathbf{X}$, see a comprehensive review in Cai (2017). One of the specifics of the problem is that the main diagonal plays a special role here because it contains relatively large variances, and in many applications all significant elements of the matrix are near the diagonal. There is no such anchor in fMRI cross-covariance matrices

because here we are typically interested in connectivity between different regions (cortices), and in general estimation of and inference for cross-covariance matrices are more involved. Nonetheless, the dramatically larger amount of statistical theory developed for covariance matrices may serve as an inspiration and the model to follow. In this section wavelet-based estimation of cross-covariance matrices is considered and an asymptotic result, matching known ones for covariance matrices, is presented. Then the next section explains the procedure of simultaneous inference with a fixed family-wise error.

To be specific in a wavelet expansion, we continue to use the plasticity example. Consider an $r$th voxel and $l$th voxel in the right and left hemispheres, respectively, and assume that we are interested in pairs $(r, l)$ from a set $\mathcal{N}$. In what follows indexes $r$ and $l$ explicitly indicate that we are dealing with voxels from the right and left hemispheres. Then, following (9), denote by $B_r(t)$ and $B_l(t)$ underlying BOLD-components of interest,

$$B_r(t) = \sum_{j=3}^{5}\sum_{k=1}^{n/2^j} \theta_{r,jk}\psi_{jk}(t), \quad B_l(t) = \sum_{j=3}^{5}\sum_{k=1}^{n/2^j} \kappa_{l,jk}\psi_{jk}(t), \tag{11}$$

and note the new notation for wavelet coefficients. Following (10) introduce empirical wavelet coefficients $\tilde{\theta}_{r,jk} = \theta_{r,jk} + n^{-1/2}\tau_r\xi_{r,jk}$ and $\tilde{\kappa}_{l,jk} = \kappa_{l,jk} + n^{-1/2}\tau_l\eta_{l,jk}$, where $\xi_{r,jk}$ and $\eta_{l,jk}$ are independent standard normal random variables. Using orthogonality of wavelet functions and the Parseval identity, we can write that the cross-covariance $\sigma_{rl}$ between $B_r(t)$ and $B_l(t)$ is

$$\sigma_{rl} := \int_0^1 B_r(t)B_l(t)dt = \sum_{j=3}^{5}\sum_{k=1}^{n/2^j} \theta_{r,jk}\kappa_{l,jk}. \tag{12}$$

Then the natural unbiased estimate of the cross-covariance is the plug-in estimate

$$\tilde{\sigma}_{rl} := \sum_{j=3}^{5}\sum_{k=1}^{n/2^j} \tilde{\theta}_{r,jk}\tilde{\kappa}_{l,jk} = \sigma_{rl} + n^{-1/2}\sum_{j=3}^{5}\sum_{k=1}^{n/2^j}(\tau_r\kappa_{l,jk}\xi_{r,jk} + \tau_l\theta_{r,jk}\eta_{l,jk} + n^{-1/2}\tau_r\tau_l\xi_{r,jk}\eta_{l,jk}). \tag{13}$$

Similarly to recent results on estimation of sparse covariance matrices, a number of interesting theoretical results, that shed light on asymptotic estimation, may be established for the cross-covariance. For instance, consider the case of a $p_1 \times p_2$ cross-covariance matrix, denote by $N_n$ the set of scales for the Bold-component of interest, and recall that in the plasticity experiment $n = 256$ and $N_{256} = \{3, 4, 5\}$. Then a hard-threshold estimator

$$\hat{\sigma}_{rl} := I\Big(|\tilde{\sigma}_{rl}| > \sqrt{2\ln(p_1p_2)}\, n^{-1/2}\hat{v}_{rl}\Big)\tilde{\sigma}_{rl}, \tag{14}$$

where $\hat{v}_{rl} := [\sum_{j\in N}\sum_{k=1}^{n/2^j}(\hat{\tau}_r^2\tilde{\kappa}_{l,jk}^2+\hat{\tau}_l^2\tilde{\theta}_{r,jk}^2)]^{1/2}$, is rate-minimax over a traditionally considered in the covariance literature class of sparse matrices and under the matrix $l_1$-norm used as a loss function. More can be found in Efromovich and Wu (2018).

The minimax property of estimator (14) sheds light on several challenges in inference for large-p-small-n cross-covariance matrices. First, even if $n$ is large (in hundreds) but estimator of $\tau$ does not take into account unfiltered physiological signals, no feasible *simultaneous* inference, for instance simultaneous confidence intervals, may be obtained for all pairs of voxels, see a discussion in Efromovich and Wu (2018). This is why accurate estimation of the level of noise is paramount. Second, it is true that in other statistical applications the sample size $n = 256$ may be considered as a large one and using the asymptotic theory becomes feasible. In fMRI data this may no longer be the case due to the following. If we return to (13), then the variance of $\tilde{\sigma}_{rl}$ is $v_{rl}^2 := \sum_{j=3}^{5}\sum_{k=1}^{n/2^j}[\tau_r^2\kappa_{l,jk}^2 + \tau_l^2\theta_{r,jk}^2] + (7/32)\tau_r^2\tau_l^2$, and we can compare it with the above-defined $\hat{v}_{rl}$ motivated by asymptotic theory. The term $(7/32)\tau_r^2\nu_l^2$ may be comparable with the double sum and hence it cannot be ignored. It will be explained shortly how to deal with this complication.

Now let us consider the problem of construction of simultaneous confidence sets for elements of the cross-correlation matrix $\rho_{rl} := \sigma_{rl}/[\sigma_{rr}\sigma_{ll}]^{1/2}$. Using (13), a plug-in estimation may be used. To get simultaneous confidence sets for the estimator, we need to understand how to evaluate large deviations for the error term on the right side of (13). As it was explained earlier, for a typical $n$ and levels of noise in fMRI data, we cannot assume that the distribution of the error term is normal. At the same time, it is possible to show that the distribution belongs to a class of sub-exponential distributions, and while this precludes us from finding close formulas for confidence sets, an exponential upper bound may be numerically computed as explained in Efromovich and Wu (2018).

We need to comment on two issues. The first one is that we declare an interhemispheric neural pathway between two voxels as active if the corresponding cross-correlation exceeds a specific threshold. In particular, Efromovich and Wu (2018) recommend the threshold 0.6, and this defines the inference procedure for a single pair of voxels. Results for other thresholds may be found in that paper. The second issue is how to propose a simultaneous inference for all $p_1 \times p_2$ pairs of voxels. Simultaneous inference is a well researched statistical

problem and a number of solutions are suggested for the case when the inference for a single test is proposed. Classical Bonferroni procedure is a standard tool, but Efromovich and Wu (2018) show that for the case of large and sparse fMRI cross-correlation matrices the more elaborate Holm procedure yields a significant edge in terms of activated pairs.

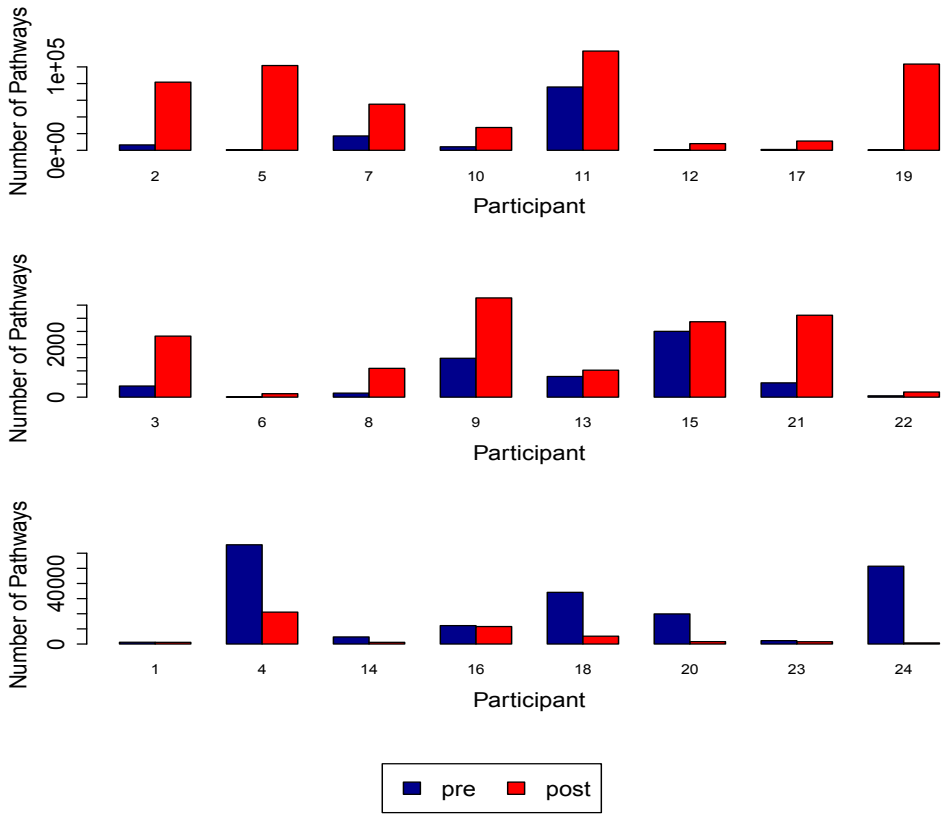


Figure 2: The number of active interhemispheric neural pathways for each participant in the neuroplasticity experiment during pre- and post-training. A neural pathway between two voxels in different hemispheres is declared as active if, with the simultaneous 0.95 degree of confidence over all considered neural pathways, the cross-correlation exceeds the threshold level 0.6.

To shed light on how the proposed simultaneous inference performs for the plasticity experiment, Figure 2 summarizes numbers of active pairs (pathways) for pre-training and post-training sessions for each of 24 participants in the neuroplasticity experiment. Here the simultaneous 0.95 degree of confidence (confidence coefficient) is used to find cross-correlations exceeding threshold 0.6. The two top rows show statistics for patients with

increased, from pre- to post-training, number of active pairs (note the different scales used in these rows). These are cases that support the neural plasticity phenomenon. The bottom row presents results for 8 participants with decreased number of active pathways. Note the large volatility in the number of active pathways among the 24 young and healthy participants. Further, Efromovich and Wu (2018) show that even during task sessions reactions of participants are remarkably different. This diversity during task fMRI sheds a new light on complexity of the problem of describing neuron networks during resting-state fMRI discussed in the next section.

# WAVELET ANALYSIS FOR RESTING-STATE fMRI

Study of functional connectivity of the human brain at rest is another active area of fMRI applications. One of the main findings is that brain regions can be synchronised in activity despite the absence of any task or stimulus. Overview of recent developments in brain structural and functional resting-state *connectomics*, including a thorough discussion of fMRI studies, may be found in Cabral, Kringelback and Deco (2017). State-of-the-art and perspectives of the dynamic functional connectomics are presented in Chen et al. (2017), Preti, Bolton and Ville (2017) and Tachmasian et al. (2017). A review of network mechanisms can be found in Mill, Ito and Cole (2017) and Liu et al. (2018), while Du, Fu and Calhoun (2018) present a review of results and new challenges in using functional connectivity for classification and prediction of brain disorders.

From statistical point of view, it is fair to say that while there are many common issues and methods in analysis of task and resting-state fMRI, the latter is more challenging due to the necessity to describe dynamically changing neural networks without underlying framework of tasks and stimulus. Further, as we know from the previos sections, BOLD signals and number of activated pairs of voxels is smaller during the rest while the level of noise is the same. Interesting discussions of task versus resting-state fMRI may be found in Di et al. (2013), Mwansisya et al. (2017), Shi et al. (2018), and Zhang S. et al. (2016).

To study dynamic functional connectivity in resting-stage fMRI, the most commonly used analytic strategy is the sliding window methodology, where the connectivity between brain

regions is computed as Pearson correlation between pairs of BOLD signals over a temporal interval spanned by a rectangular window. This computation is repeated iteratively by shifting the window by a specific step every time, see Mill, Ito and Cole (2017). Building on this core framework, improvements in several directions have been developed: (i) Using different window types (kernel functions); (ii) A frame-wise analysis where only moments when the BOLD signal exceeds a threshold are retained for the analysis, and using temporal modeling, see Preti, Bolton and Van De Ville (2017); (iii) Activity in a set of regions of interest is modeled using a multivariate Gaussian distribution with a mean vector and covariance matrix that are allowed to vary as the experiment progresses. As the computation of the covariance matrix might be difficult, imposing sparsity is recommended and a corresponding discussion may be found in Xu and Lindquist (2015) and Wee et al. (2016b); (iv) Using of regularization strategy to the precision matrix, the inverse of the covariance matrix, is discussed in Allen et al., 2014, Wee et al. (2016) and Marusak et al. (2017). Further, conditional rather than marginal independence may be enforced by limiting the amount of non-zero coefficients of the precision matrix, which is expected to be particularly useful when the number of observations (time points) at each node are limited, see Xu and Lindquist (2015). Among other statistical methods used in data-driven classification and prediction, let us mention spatial independent component analysis, independent vector analysis, support vector machines, linear discriminant analysis, and artificial neural network, see a review in Du, Fu and Calhoun (2018).

Wavelet analysis, as it could be expected, has been extensively used in resting-state fMRI studies, see a discussion and reviews in Smith et al. (2015), Patel and Bullmore (2016), Zhang Z. et al. (2016) and Skidmore et al. (2017). Let us point upon some specifics in the resting-state wavelet analysis. A majority of wavelet studies are done not using DWT but maximal overlap discrete wavelet transform (MODWT), which is also may be found in the literature under names undecimated (or nondecimated) DWT, stationary DWT, translation (or time) invariant DWT, and redundant DWT, see Percival and Walden (2000). The main attractive feature of MODWT for analysis of resting-state fMRI is that unlike the DWT, MODWT is defined naturally for all samples sizes and not just dyadic. Further, MODWT forms multiresolution analyses and preserves wavelet power spectrum under circular shifts.

Further, MODWT is supported by all main wavelet software packages. Its drawback is that MODWT is not orthonormal and highly redundant. Further, theoretically we know dramatically less about statistical estimation and inference for MODWT, and this is an interesting area of future research. At the same time, let us point upon empirical study in Zhang, Z. et al. (2016) that compares using DWT and MODWT in a resting-state experiment for 29 healthy controls and 29 participants with chronic schizophrenia. The authors conclude that in detecting differences between the two groups, MODWT produces more stable results.

It is an open and interesting problem to expand the above-presented theoretical task-fMRI results to resting-state fMRI. Another open and challenging problem is to use wavelet analysis for solving change point resting-state problems discussed in Xu and Lindquist (2015).

# CONCLUSION

The article reviews rapidly emerging fMRI wavelet applications in statistical analysis of the dynamic functional networks of the human brain with a great potential to treat a number of brain diseases. Functional magnetic resonance imaging is a powerful tool that may allow us to analyze brain activity on a voxel level, but it is fair to say that this opportunity is often skipped due to Big Data problem and large fMRI noise, and instead averaging over large areas of interest is used. Wavelet analysis allows to resolve these issues and then study functional networks on a voxel-to-voxel level. It is explained how wavelets help to solve the problem of data reduction, filtering noise, estimation of and inference for large-p-small-n matrices. In short, rephrasing the Voltaire's "Si Dieu n'existait pas, il faudrait l'inventer," we may say that if wavelets did not exist, it would be necessary to invent them for fMRI.

Functional connectivity in the brain is studied via both task and resting-state fMRI experiments. The latter presents its own challenges due to lower signal-to-noise ratio and the necessity to follow the dynamic of functional connectivity in the absence of any task or stimulus. As a result, even different wavelet transforms are recommended, and a problem of finding change points becomes a central one. It is also fair to conclude that the theory of wavelet analysis for resting-state fMRI is less developed and there is a growing need in its development and making it on par with the wavelet theory for the task fMRI.

Despite a great progress in improving the fMRI technology and creating smart softwares for decreasing physiological and movement noise, this noise is still the main obstacle in statistical analysis of fMRI data. The article explains how a standard regression procedure, which exploits the presence of physiological noise, helps to estimate empirical wavelet noise.

The final remark is about future research. If the reader is thinking about joining researchers working on fMRI applications, it is a right time to do this. From statistical point of view, there are many interesting and open problems about efficient estimation of and inference for maximal overlap discrete wavelet transform, or how to translate the emerging family of theoretical results on estimation of large-p-small-n covariance/correlation matrices proposed for analysis of microarrays into corresponding ones for fMRI. Simultaneous statistical inference for hundreds of thousands pairs of voxels and developing the theory of change point and sequential sampling are other attractive areas of research. Further, evolving fMRI experiments create new statistical challenges. As an example, the article reviews results of the neuroplasticity experiment for 24 healthy participants where everyone exhibited his own personality with sometimes dramatic differences in reaction to the same tasks and stimulus. This is what makes the problem of exploring the human brain so challenging and, keeping in mind the potential for the treatment of brain diseases, so rewarding. Wavelets is an excellent tool for analysis of fMRI, and they also may be used for analysis of electroencephalography (EEG) and magnetoencephalography (MEG), see a discussion and reviews in Bruns (2004), Muthukumaraswamy and Johnson (2004), Kiebel et al. (2005), Liao et al. (2013), Faust et al. (2015), El-Samie (2018), Ishii et al. (2018), and van Viet et al. (2018). Functional wavelet analysis of fMRI, EEG and MEG is another attractive topic of research, see Raz and Turetsky (1999) and Morettin, Pinhero and Vidakovic (2017).

# ACKNOWLEDGEMENTS

The research was supported in part by NSF Grant DMS-1513461. Suggestions of the editors and referees are greatly appreciated.

# REFERENCES


Addison, P. (2005). Wavelet transforms and the ECG: a review. *Physiological Measurement*, 26, 155-199.

Albert, N., Robertson, E. and Miall, C. (2014). The resting human brain and motor learning. *Current Biology*, 19, 1023-1027.

Allen, E.A., Damaraju, E., Plis, S.M., Erhardt, E.B., Eichele, T., Calhoun, V.D. (2014). Tracking whole-brain connectivity dynamics in the resting state. Cerebrial Cortex, 24 663-676.

Anderson, J. et al. (2010). Decreased interhemispheric functional connectivity in autism. *Cerebral cortex* 21, 1134-1146.

Ashby, G. (2011). *Statistical Analysis of fMRI Data*. Cambridge: The MIT Press.

Barrett, K., Barman, S., Boitano, S., & Brooks, H. (2016). *Ganong's Review of Medical Physiology*. New York: McGraw-Hill.

Bassett D., et al. (2011). Dynamic reconfiguration of human brain networks during learning. *Proc Natl Acad Sci USA*, 108,7641-7646.

Bassett, D. & Sporns, O. (2017). Network neuroscience. *Nature neuroscience* 20, 353-364.

Birn, R. (2012). The role of physiological noise in resting-state functional connectivity. *Neuroimage*, 62(2), 864-870.

Biswal, B. et al. (1995). Functional connectivity in the motor cortex of resting human brain using echo airplanar mri. *Magnetic Resonance in Medicine*, 34, 537-541.

Bruns, A. (2004). Fourier-, Hilbert- and wavelet based signal analysis: are they really different approaches? *Journal of Neuroscience Methods* 132, 321-332.

Caballero-Gaudes, C., & Reynolds, R. C. (2017). Methods for cleaning the BOLD fMRI signal. *Neuroimage*, 154, 128-149.

Cabral, J., Kringelbach, M., & Deco, G. (2017). Functional connectivity dynamically evolves on multiple time-scales over astatic structural connectome: Models and mechanisms, *NeuroImage* 160, 84-96.

Cai, T. T. (2017). Global testing and large-scale multiple testing for high-dimensional covariance structures. *Annual Review of Statistics and Its Applications*, 4, 423-446.

Casella, G., & Berger, R. (2002). *Statistical Inference*, 2nd ed. New York: Duxbury.

Chang, C., & Glover, G. (2009). Effects of model-based physiological noise correction on default mode network anti-correlations and correlations. *Neuroimage*, 47(4), 1448-1459.

Chen, L. et al. (2017). Biophysical and neural basis of resting state functional connectivity: Evidence from non-human primates. *Magnetic Resonance Imaging*, 39, 71-81.

Di, X., Gohel, S., Kim, E., & Biswal, B. (2013). Task vs. rest – different network configurations between the coactivation and the resting-state brain networks. *Frontiers In Human Neuroscience*, 7, 1-9.

Dimyan, M. , & Cohen, L. (2011) Neuroplasticity in the context of motor rehabilitation after stroke. *Nature Reviews Neurology*, 7(2), 76-85.

Du, Y., Fu, Z., & Calhoun, V. (2018). Classification and Prediction of Brain Disorders Using Functional Connectivity: Promising but Challenging. *Frontiers in Neuroscience*, 12(525), 1-10.

Efromovich, S. (1999a). *Nonparametric Curve Estimation: Methods, Theory and Applications.* New York: Springer.

Efromovich, S. (1999b). Quasi-linear wavelet estimation. *Journal of the American Statistical Association*, 94, 189-204.

Efromovich, S., & Valdez-Jasso, Z. (2010). Aggregated wavelet estimation and its applications to ultra-fast fMRI. *Journal of Nonparametric Statististics*, 22, 841-857.

Efromovich, S., & Smirnova, E. (2014). Statistical analysis of large cross-covariance and cross-correlation matrices produced by fMRI images. *Journal of Biometric Biostatistics*, 5, 1-8.

Efromovich, S. (2018). *Missing and Modified Data in Nonparametric Estimation.* New York: CRC Press.

Efromovich, S., & Wu, J. (2018). Wavelet analysis of Big Data contaminated by large noise in an fMRI study of neuroplasticity *Methodology and Computing in Applied Probability*, 20, 1381-1402.

El-Samie, F. et al. (2018). A review of EEG and MEG epileptic spike detection algorithms. *IEEE Access*, 6, 60673 - 60688.

Fan, J., Han, F., & Liu, H. (2014). Challenges in Big Data analysis. *National Science Review*, 1, 293-324.

Faivre, A. AudreyRicoac, A., Zaaraouia, W., Reuterac, F., Confort-Gounya, S., Guyead, M., Pelletierac, J., Ranjevaa, J., & Audoinac, B. (2015). Brain functional plasticity at rest and during action in multiple sclerosis patients. *Journal of Clinical Neuroscience* 22, 1438-1443.

Faust, O., Acharya, U., Adeli, H. and Adeli, A. (2015). Wavelet-based EEG processing for computer-aided seizure detection and epilepsy diagnosis. *Seizure*, 26, 56-64.

Ganong, William F., and Kim E. Barrett ( 2005). *Review of medical physiology.* New York:

McGraw-Hill Medical.

Goni, J. et al. (2014). Resting-brain functional connectivity predicted by analytic measures of network communication. *Proc Natl Acad Sci USA*, 111, 833-838.

Honey, C., Kotter, R., Breakspear, M. and Sporns, O. (2007). Network structure of cerebral cortex shapes functional connectivity on multiple time scales. *Proc Natl Acad Sci USA*, 104, 10240-10245.

He, H., & Liu, T. (2012). A geometric view of global signal confounds in resting state functional MRI. *Neuroimage* 59(3), 2339-2348.

Henson, R. et al. (1999). The slice-timing problem in event-related fMRI. *NeuroImage*, 9, 125.

Ishii R, Pascual-Marqui, R., Canuet, L., Xiang, J. and Gaetz, W. (2018) Editorial: New insights on basic and clinical aspects of EEG and MEG connectome. *Front. Hum. Neurosci.* 232. doi: 10.3389/fnhum.2018.00232

Kelly, C. et al. (2011). Reduced interhemispheric resting state functional connectivity in cocaine addiction. *Biological psychiatry*, 69, 684-692.

Kiebel, S. et al. (2007). Dynamic causal modeling: a generative model of slice timing in fMRI. *Neuroimage* 1487-1496.

Laird, A., Fox, P., Khazaie, H., Zarei, M., Eggers, C., & Eickhoff, C. (2017). Resting-state functional reorganization in Parkinson's disease: An activation likelihood estimation meta-analysis. *Cortex* 92, 119-138.

Lazar, N. (2008). *The Statistical Analysis of Functional MRI Data*, New York: Springer.

Lindquist, M. (2008). The Statistical Analysis of fMRI Data. *Statistical Science*, 23, 439-464,

Logothetis, N., Pauls, J., Augath, M., Trinath, T., & Oeltermann, A. (2001). Neuro-physiological investigation of the basis of the fMRI signal. *Nature*, 412, 150-157.

Liao, K., Zhu, M. and Ding, L. (2013). A new wavelet transform to sparsely represent cortical current densities for EEG/MEG inverse problems. *Comput Methods Programs Biomed*, 111, 376-388.

Liu, X., Zhang, N., Chang, C., & Duyn, J. (2018). Co-activation patterns in resting-state fMRI Signals, *Neuroimage*, in press.

Logothetis, N., Pauls, J., Augath, M., Trinath, T., & Oeltermann, A. (2001). Neuro-physiological investigation of the basis of the fMRI signal. *Nature*, 412, 150-157.

Marusak, H., Calhoun V., Brown, S., Crespo,L., Sala-Hamrick, K., Gotlib, I., & Thomason M. (2017), Dynamic functional connectivity of neurocognitive networks in children. *Human*

*Brain Mapping* 38, 97-108.

Mill, R., Ito, T., & Cole, M. (2017). From connectome to cognition: The search for mechanism in human functional brain networks, *NeuroImage*, 160, 124-139.

Morettin, P, Pinhero, A. and Vidakovic, B. (2017). *Wavelets in Functional Data Analysis.* New York: Springer.

Mill, R. et al. (2017). Empirical validation of directed functional connectivity, *Neuroimage*, 146, 275-287.

Misic, B. and Sporns, O. (2016). From regions to connections and networks: new bridges between brain and behavior. *Curr. Opin. Neurobiol.*, 40, 1?7.

Murphy, K., Birn, R., & Bandettini, P. (2013). Resting-state fMRI confounds and cleanup. *Neuroimage*, 80, 349-359.

Muthukumaraswamy, S. and Johnson, B. (2004). Primary motor cortex activation during action observation revealed by wavelet analysis of the EEG. *Clinical Neurophysiology*, 115, 1760-1766.

Nason, G. (2008). *Wavelet Methods in Statistics with R.* New York: Springer.

Ogden, T. (1997). *Essential Wavelets for Statistical Applications and Data Analysis.* Basel: Birkhäuser.

Ozmen, G., & Ozsen, S. (2018). A new denoising method for fMRI based on weighted three-dimensional wavelet transform *Neural Computing and Applications*, 29, 263-276.

Papoutsi, M., Weiskopf, N., Langbehn, D., Reilmann, R., Rees, G., & Tabrizi, S. J. (2018). Stimulating neural plasticity with real-time fMRI neurofeedback in Huntington's disease: A proof of concept study. *Human Brain Mapping*, 39, 1339-1353.

Pantano, P., Petsas, N., Tona, F., & Sbardella, E. (2015). The role of fMRI to assess plasticity of the motor system in MS. *Frontiers in Neurology*, 6, 1-5.

Patel, A., & Bullmore. E. (2016). A wavelet-based estimator of the degrees of freedom in denoised fMRI time series for probabilistic testing of functional connectivity and brain graphs. *NeuroImage*,142, 14-26.

Percival, D., & Walden, A. (2000). *Wavelet Methods for Time Series.* Cambridge: Cambridge Univ. Press.

Preti, M., Bolton, T., & Van De Ville, D. (2017). The dynamic functional connectome: State-of-the-art and perspectives. *NeuroImage*, 160, 41-54.

Raz, J. & Turetsky, B. (1999). Wavelet ANOVA and fMRI. *Proc. SPIE 3813, Wavelet Applications in Signal and Image Processing VII*, doi:10.1117/12.36681.

Sladky, R. et al. (2011). Slice-timing effects and their correction in functional MRI. *Neuroimage*, 58, 588-594.

Sporns, O. (2014). Contributions and challenges for network models in cognitive neuroscience. *Nat. Neuroscience*, 17, 652-660.

Tahmasian, M. et al. (2007). Brain Plasticity and fMRI, 209-226. In: Stippich C. (eds) *Clinical Functional MRI. Medical Radiology (Diagnostic Imaging)*. Berlin: Springer.

Thomas, C. et al. (2014). Anatomical accuracy of brain connections derived from diffusion MRI tractography is inherently limited. *Proc Natl Acad Sci USA*, 111, 16574-16579.

Shi, L., Sun, J.,Xia, Y., Ren, Z., Chen, Q., Wei, D., Yang, W., & Qiu, J. (2018). Biological Psychology Large-scale brain network connectivity underlying creativity in resting-state and task fMRI: Cooperation between default network and frontal-parietal network. *Biological Psychology*, 135, 102-111.

Sharma, N., Classen, J., & Cohen, L. (2013). Neural plasticity and its contribution to functional recovery. Handbook of Clinical *Neurology*, 110, 3?12.

Skidmore, F., Korenkevych, D., Liu, Y., He, G., Bullmore, E., & Pardalos, P. (2011). Connectivity brain networks based on wavelet correlation analysis in Parkinson fMRI data, *Neuroscienced Letters*, 499: 47-51.

Smith, R., Jann, K., Ances, B., & Wang, D. (2015). Wavelet-based regularity analysis reveals recurrent spatiotemporal behavior in resting-state fMRI. *Human Brain Mapping* 36: 3603-3620.

Tung, K. et al. (2013). Alterations in resting functional connectivity due to recent motor task *Neuroimage*, 78, 316-324.

Valdez-Jasso, Z. (2010). Aggregated wavelet estimation with applications. PhD Thesis, UTDallas, Richardson.

Vidakovic, B. (1999). *Statistical Modeling by Wavelets*. New York: Wiley.

Wee, C.-Y., Yap, P.-T., & Shen, D. (2016). Diagnosis of autism spectrum disorders using temporally distinct resting-state functional connectivity networks. *CNS Neuroscience and Therapeutics*, 22, 212-219.

Weissenbacher, A. et al. (2009). Correlations and anticorrelations in resting-state functional connectivity MRI: a quantitative comparison of preprocessing strategies. *Neuroimage*, 47(4), 1408-1416.

Welvaert, M. et al. (2011). neuRosim: An R package for generating fMRI data. *Journal of Statistical Software*, 44, 1-18.

Welvaert, M. and Rosseel, Y. (2013). On the definition of signal-to-noise ratio and contrast-to-noise ratio for fMRI data. *PLOSONE*, 8(11), 1-10.

Xu, Y., & Lindquist, M.A. (2015). Dynamic connectivity detection: an algorithm for determining functional connectivity change points in fMRI data. *Frontiers in Neuroscience*, 9, 1-19.

Xue, Z., Fengd, J., & Liu, Z. (2017). Task and resting-state fMRI studies in first-episode schizophrenia: A systematic review. *Schizophrenia Research*, 189, 9-18.

Zalesky, A., Fornito, A. and Bullmore, E. (2012). On the use of correlation as a measure of network connectivity. *Neuroimage*, 60, 2096?2106.

Zhang S, Li X, Lv J, Jiang X, Guo L., & Liu T. (2016), Characterizing and Differentiating Task-based and Resting State FMRI Signals via Two-stage Sparse Representations. *Brain Imaging and Behavior*, 10, 21-32.

Zhang Z., Telesford Q., Giusti C., Lim K., & Bassett, DS (2016). Choosing Wavelet Methods, Filters, and Lengths for Functional Brain Network Construction. *PLoS ONE*, 11, 1-24.